Generalized *q*-plates and alternative kinds of vector and vortex beams

Martin Vergara* and Claudio Iemmi

Facultad de Ciencias Exactas y Naturales, Departamento de Física, Universidad de Buenos Aires, Buenos Aires, Argentina and Consejo Nacional de Investigaciones Científicas y Técnicas, Buenos Aires, Argentina

(Received 21 December 2018; published 6 November 2019)

We took a generalization of the conventional concept of the *q*-plate, allowing in its definition nonlinear functions of the azimuthal coordinate, and simulated the resulting fields of applying this kind of element to uniformly polarized input beams, both in the near-field (Fresnel diffraction) and the far-field (Fraunhofer diffraction) approximations. In general terms, when working in the near-field regime, the chosen function defines the output polarization structure for linearly polarized input beams and the phase of the output field for circularly polarized input beams. In the far-field regime, it is obtained that when there are nonlinearities in the azimuthal variable, the central singularity of the polarization field of a vector or vortex beam may divide into several singularities of lower topological charge, preserving the total charge. Depending on the chosen *q*-plate function, different particular behaviors on the output beam are observed, which offers a whole range of possibilities for creating alternative kinds of vector and vortex beams, as well as polarization critical points and singularity distributions.

DOI: 10.1103/PhysRevA.100.053812

I. INTRODUCTION

Vector beams are known for showing a nonuniform distribution of the state of polarization (SoP) [1]. The most common beams of this kind are radially and azimuthally polarized beams, particular cases of cylindrical vector beams [2], in which the SoP varies linearly with the azimuthal coordinate θ. Vector beams have been widely studied because of their tight-focusing properties [3]. Besides, they have potential application to communications [4], optical tweezers and particle micromanipulation [5–8], material processing [9], quantum entanglement [10], and more.

There are many methods for creating vector beams, generally divided into two categories, active and passive. Active methods consist of modifying the resonant cavity of a laser for obtaining an output vector beam, while passive ones aim to modulate the wave front of a conventional laser beam with suitable optical elements [1]. In the latter case *q*-plates have become a convenient choice [11].

A conventional *q*-plate works as a half-wave plate in which the director axis rotates as the linear function $q\theta$ of the azimuthal coordinate θ [12–14]. Its matrix representation in the Jones formalism has the form

$$M_q(\theta) = \begin{pmatrix} \cos(2q\theta) & \sin(2q\theta) \\ \sin(2q\theta) & -\cos(2q\theta) \end{pmatrix}. \tag{1}$$

When a linearly polarized beam passes through such an element, it becomes a vector beam with a structured polarization pattern in which the azimuth of the polarization ellipses varies as the function $2q\theta$, reaching a total rotation of $4q\pi$. On the other hand, when impinging with a circularly polarized beam, the spin to orbital conversion (STOC) phenomenon takes place: the orbital angular momentum (OAM) of the beam varies according to $\Delta l = \pm 2q$, where the plus sign applies when impinging with left circular polarization and the minus sign when impinging with right circular polarization. In other words, if a uniform left circularly polarized beam (total angular momentum of $+1$) passes through a *q*-plate, it becomes a uniform right circularly polarized vortex beam with an OAM charge $l = 2q$ [total angular momentum variation of $2(q-1)$]. The value $2q$, which gives the times the polarization vector (or phase) completes a 2π turn along the azimuth coordinate, is known as the topological charge.

This way *q*-plates are high versatile elements, with many potential applications in the field of singular optics, since they allow alternately the creation of phase singularities (vortex beams with OAM) and polarization singularities (vector beams). Additionally, the possibility of using spatial light modulators (SLM), like liquid crystal displays which allow pixel to pixel phase only modulation [15,16], for the implementation of these devices gives great flexibility for designing alternative kinds of vector and vortex beams. It easily allows extending the concept of the *q*-plate, including modulations of the polarization field that are not necessary linear in θ.

Recently there have been advances towards this direction, creating *q*-plates with different q values depending on the region of the element [17], with nonlinear functions of θ for binary codification [18] or with radial dependence for creating high-order Laguerre-Gaussian beams [19].

In this paper we simulate an element that arises from generalizing the concept of the *q*-plate, allowing arbitrary (not necessary linear) modulations of the polarization field of a beam, in such a way that we are able to explore complex beams, with alternative kinds of polarization structures and singularity distributions, and study their propagation properties.

*marto@df.uba.ar

The Jones matrix that describes this generalized q-plate is

$$M_\Phi(\theta) = \begin{pmatrix} \cos(2\Phi(\theta)) & \sin(2\Phi(\theta)) \\ \sin(2\Phi(\theta)) & -\cos(2\Phi(\theta)) \end{pmatrix}, \tag{2}$$

and it represents a half-wave plate in which the director axis angle is an arbitrary function, $\Phi(\theta)$. The only requirement we impose is that Φ is a continuous periodic function in θ, with the period $\tau = 2\pi/n$, with n being any integer number.

The infinite possible choices of the function Φ and the flexibility in their implementation provided by the use of SLMs make the generalized q-plate a tool with great potential in the field of beam tailoring, allowing further research of new effects and focusing properties of alternative kinds of vector and vortex beams. Here we demonstrate the creation of two types of beams using this technique, for the purpose of illustrating with simple cases the effect of focusing nonlinear distributions of polarization and phase, with and without net topological charge.

In Sec. II we simulate generalized q-plates with nonlinear dependence in the azimuthal coordinate, showing its effect on the intensity, phase, and polarization distributions of a uniform circular section input beam (top hat beam), for different polarizations. We show the resulting fields in both the near-field and the far-field approximations and give an explanation of these results based on Fourier analysis. We outline in Sec. III a proposal for an experimental implementation using a reflective liquid crystal display (LCoS) with phase-only modulation. The main conclusions are given in Sec. IV.

II. NONLINEAR GENERALIZED q-PLATES IN THE AZIMUTHAL VARIABLE

When the function Φ grows nonlinearly in the azimuthal coordinate θ, a variety of interesting effects can be observed over the resulting field's amplitude, phase, and polarization structure; in this section we show some examples of the different behaviors found.

We chose these simple examples for illustrating the effect of nonlinearity, one changing the growth power of the azimuthal phase without changing the total modulation and the other setting up a nonlinear modulation that leaves null the net topological charge.

A. Polynomial growth

We have simulated a plate defined by the nonlinear function $\Phi(\theta) = q(2\pi)^{(1-p)}\theta^p$. The multiplicative constant $(2\pi)^{(1-p)}$ is due to the continuity condition: $\Phi(2\pi) = q2\pi$, meaning that the total azimuthal variation is q times 2π, without discontinuous steps in Φ after a 2π period in θ. Figure 1 shows some examples of the simulated argument function of these plates $[2\Phi(\theta)]$ for different powers of p and values of q. The total azimuthal variation of the argument function is given by $2q$ times 2π, which defines the topological charge of the created beams, as will be seen soon. These beams illustrate in a simple way the effect of breaking linearity in the q-plate element, in both in near- and far-field propagation.

We studied how these generalized q-plates affect an input beam with uniform phase and intensity within a circular profile (top-hat beam), simulating both the obtained field just after passing through the plate and that obtained in the far-field approximation, i.e., the Fraunhofer diffraction of the former. For a vector field, this is performed simply by computing the Fourier transform of each of the $\hat{x}$ and $\hat{y}$ components of the field [20],

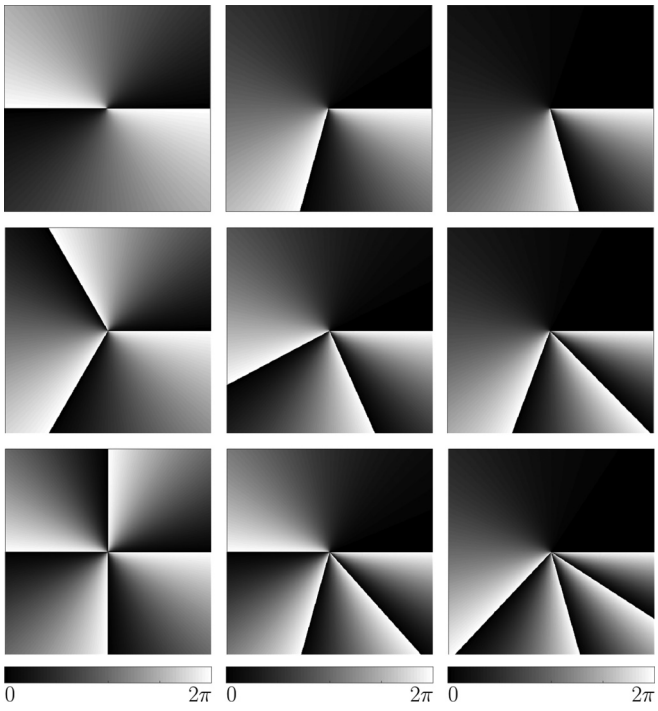

FIG. 1. Argument phase function of the generalized q-plates determined by a polynomial growth in θ. The first, second, and third columns show the cases for powers $p = 1$, $p = 2$, and $p = 3$, respectively, while the first, second, and third rows show the cases for topological charges $q = 1$, $q = 3/2$, and $q = 2$, respectively.

$$\mathcal{F}\{\mathbf{E}(x,y)\} = \tilde{\mathbf{E}}(u,v) = \begin{pmatrix} \tilde{E}_s(u,v) \\ \tilde{E}_p(u,v) \end{pmatrix} = \begin{pmatrix} \mathcal{F}\{E_s(x,y)\} \\ \mathcal{F}\{E_p(x,y)\} \end{pmatrix}. \tag{3}$$

This is implemented numerically by means of the two-dimensional discrete Fourier transform of an $N \times N$ matrix, where each element is the corresponding value of the electric field $\mathbf{E}(x,y)$ after passing through the generalized q-plate.

Figure 2 shows the intensity and polarization distribution, as well as the azimuth of the polarization ellipses, at the output plane of the generalized q-plate (the last one is represented with a gray scale from $-\pi/2$ to $\pi/2$) for powers $p = 1$ and $p = 2$, and different values of q, when the input beam is linearly polarized in the vertical direction. The azimuth of the polarization ellipses is obtained by computing the phase of the complex Stokes field $S_{12}(x,y) = S_1(x,y) + iS_2(x,y)$, where $S_i(x,y)$ are the Stokes parameters of the electric field [21].

In the case when $p = 1$ (linear q-plate) and $q = 1/2$ an azimuthally polarized vector beam is obtained, whose topological charge is determined by the number of times that the polarization vector gives a complete turn around the beam axis [16] (in this case $2q = 1$). When increasing the power to

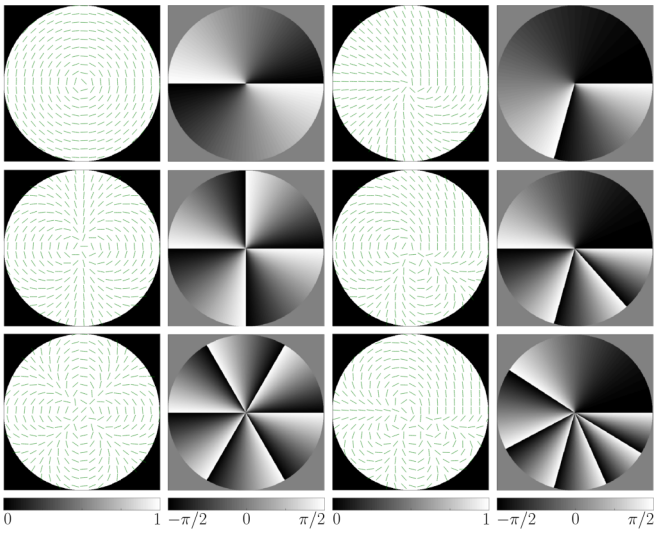

FIG. 2. Polarization ellipses and their azimuths resulting from input vertical polarization for polynomial generalized q-plates. The first and third columns show intensity and polarization ellipses for $p = 1$ and $p = 2$, respectively. The second and fourth columns show polarization azimuths for $p = 1$ and $p = 2$, respectively. The first, second, and third rows show cases with topological charges $q = 1/2$, $q = 1$, and $q = 3/2$, respectively. The output consists of vector beams in which the azimuth grows accordingly to the power p.

$p = 2$ the topological charge does not change, while the cylindrical symmetry is lost, since the azimuth grows quadratically with θ. The same behavior is seen for higher topological charges.

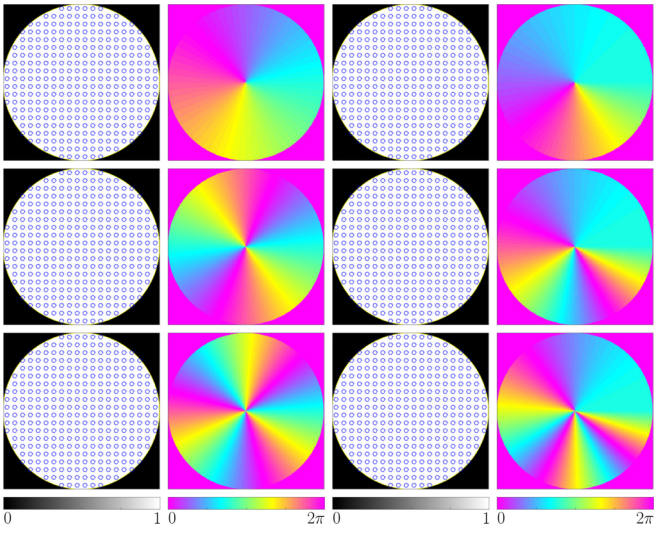

FIG. 3. Polarization ellipses and phase distributions resulting from input left circular polarization for polynomial generalized q-plates. The first and third columns show intensity and polarization ellipses for $p = 1$ and $p = 2$, respectively. The second and fourth columns show the phase for $p = 1$ and $p = 2$, respectively. The first, second, and third rows show cases with topological charges $q = 1/2$, $q = 1$, and $q = 3/2$, respectively. The output consists of uniformly right circular polarized beams in which the phase grows accordingly to the power p.

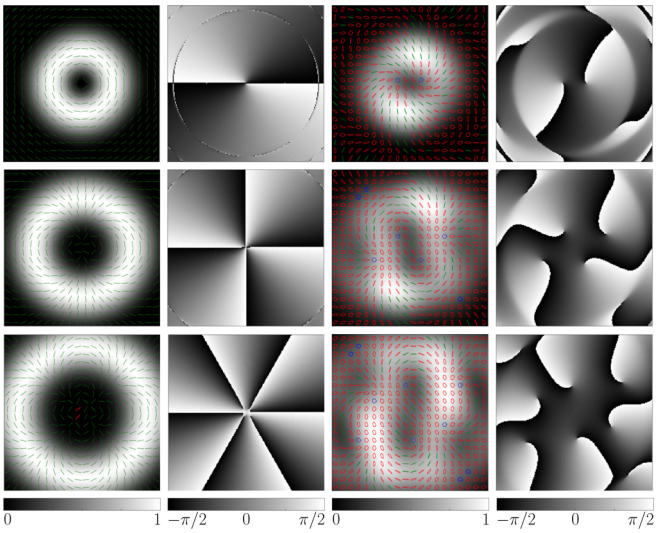

FIG. 4. Polarization ellipses and their azimuths resulting from input vertical polarization for polynomial generalized q-plates, in the far-field regime. The first and third columns show the intensity distribution and the polarization structure for $p = 1$ and $p = 2$, respectively. The second and fourth columns show the azimuths of the polarization ellipses for $p = 1$ and $p = 2$, respectively. The first, second, and third rows show the cases for $q = 1/2$, $q = 1$, and $q = 3/2$, respectively.

In Fig. 3 the behavior of these elements when they are illuminated with circularly polarized light is analyzed. In this case the polarization ellipse fields and the beam phase distributions are shown. We choose (from now on) to represent these magnitudes because, as a general fact for q-plates, when input polarization is linear, the modulation occurs in the polarization field, but when input polarization is circular, it occurs in the phase of the field, while the polarization remains uniform, with the opposite sense of rotation due to the STOC phenomenon.

As it was previously said, for input left circular polarization the STOC phenomenon, giving place to a output uniform right circularly polarized beam, carrying OAM with the topological charge $l = 2q$ was observed. This was seen in the 2π turn of the beam phase around the propagation axis. The way the phase grows depends on the power p.

An interesting effect arises when the Fraunhofer diffraction patterns of these beams are calculated. Figure 4 shows the result from propagating the output beams obtained when impinging with linear vertical polarization (Fig. 2). Both, the polarization ellipses superposed to the intensity distribution and the azimuths of the ellipses are represented. In order to plot the polarization ellipses we used a color code based on the respective form factor $f = b/a$, the ratio between the minor b axis and the mayor a axis of the ellipse, whose sign depends on the vector sense of rotation (negative for right-handed and positive for left-handed). There is a neighborhood around $f = 0$ for which we considered polarization to be linear (green) and neighborhood around $f = \pm 1$ for which we considered polarization to be circular (blue); in any other case the polarization is elliptical (red).

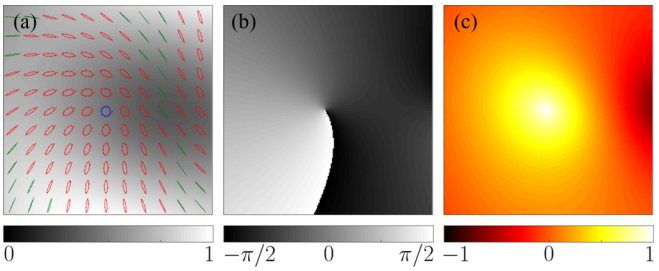

FIG. 5. Zoom of one of the polarization singularities obtained in the far field for a polynomial generalized q-plate with $q = 1/2$ and $p = 2$, when the input polarization is vertical. (a) Intensity and polarization ellipses. (b) Azimuth of the polarization ellipses. (c) Form factor of the polarization ellipses.

For linear q-plates ($p = 1$) the polarization field in the Fraunhofer regime is the same as that in the q-plate plane, with a "donut" intensity distribution, due to the central polarization vortex [11]. Conversely, the beams obtained from nonlinear generalized q-plates do not preserve their polarization fields; nonlinearities break the cylindrical symmetry of the SoP and intensity distributions. It can be seen that, instead of showing a central singularity with a topological charge of $2q$, they show $4q$ isolated singularities, each one with a topological charge of $1/2$, adding up to a total charge of $2q$. Furthermore, the nature of these singularities differs from the original dark singularity. In Fig. 5 this fact is shown in detail for one of these singularities. It can be seen that the azimuth is not defined in these points, although the form factor is and is at maximum (left circular polarization). These singularities are generally known as C-points: isolated points of circular polarization around which polarization azimuth rotates in $m2\pi$. The topological charge in these cases is $m = 1/2$.

Figure 6 shows the Fraunhofer diffraction of the beams obtained when impinging onto the generalized q-plates with left circularly polarized light. In this case, for a linear q-plate, the phase and polarization distributions are identical to those seen in the q-plate plane, with a central singularity (phase vortex) with the topological charge $2q$, due to the creation of OAM. In the nonlinear case, $2q$ isolated vortices with a topological charge of 1 appear, occupying the same position as half of the C-points obtained in the case of linearly polarized light (Fig. 4). If impinging with right circularly polarized light (not shown), there would be another $2q$ vortex, located according to the other half of the C-points. These nonuniform intensity and phase gradients may give rise to optical force fields applicable to optical trapping and micromanipulation [22].

This singularity splitting can be explained in terms of the far-field (Fraunhofer) diffraction phenomenon. The Fraunhofer field coincides with the Fourier transform of the field at the generalized q-plate plane, which [for the function $g(r, \theta)$ separable in polar coordinates] can be written in terms of an infinite sum of weighted Hankel transforms [23],

$$\mathcal{F}\{g(r,\theta)\} = \sum_{k=-\infty}^{\infty} c_k (-i)^k e^{ik\phi} \mathcal{H}_k\{g_R(r)\}, \tag{4}$$

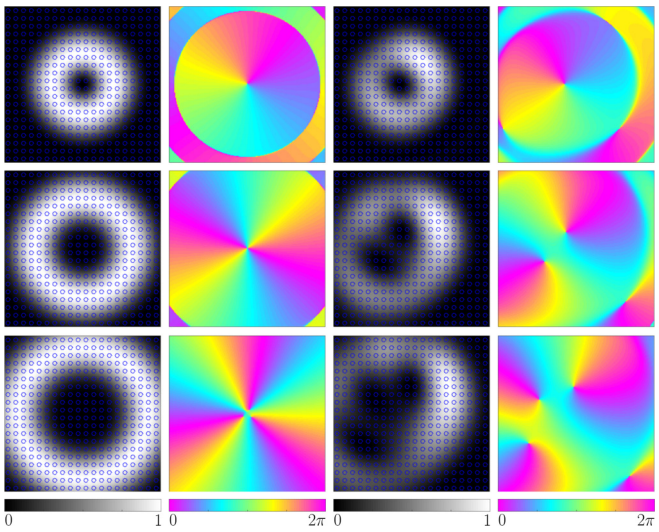

FIG. 6. Polarization ellipses and phase distribution resulting from an input beam with left circular polarization for polynomial generalized q-plates, in the far-field regime. The first and third columns show the intensity distribution and polarization structure for $p = 1$ and $p = 2$, respectively. Polarization is in every case uniform right circular. The second and fourth columns show the phase of the field for $p = 1$ and $p = 2$, respectively. The first, second, and third rows show the cases for $q = 1/2$, $q = 1$, and $q = 3/2$, respectively.

where

$$c_k = \frac{1}{2\pi} \int_0^{2\pi} g_\Theta(\theta) e^{-ik\theta} d\theta \tag{5}$$

and $\mathcal{H}_k$ is the Hankel transform operator of order k,

$$\mathcal{H}_k\{g_R(r)\} = 2\pi \int_0^{\infty} r g_R(r) J_k(2\pi r\rho) dr, \tag{6}$$

with J_k being the kth-order Bessel function of the first kind, and $g(r, \theta) = g_R(r) g_\Theta(\theta)$.

With this in mind we can take as an example the cases shown in Fig. 2 for $q = 1/2$ and calculate the weight distributions in each case. In the linear case ($p = 1$), when the input light is vertically polarized, the electric field after the q-plate is obtained from Eq. (2) as

$$\begin{aligned} \mathbf{E}_o(r,\theta) &= M_\Phi(r,\theta)\mathbf{E}_i(r,\theta) \\ &= \begin{pmatrix} \cos(\theta) & \sin(\theta) \\ \sin(\theta) & -\cos(\theta) \end{pmatrix} \begin{pmatrix} 0 \\ E_i \end{pmatrix} \\ &= E_i \begin{pmatrix} \sin(\theta) \\ -\cos(\theta) \end{pmatrix} = \begin{pmatrix} E_s(r,\theta) \\ E_p(r,\theta) \end{pmatrix}, \end{aligned} \tag{7}$$

while in the nonlinear case with $p = 2$,

$$\mathbf{E}_o(r,\theta) = \begin{pmatrix} E_s(r,\theta) \\ E_p(r,\theta) \end{pmatrix} = E_i \begin{pmatrix} \sin\left(\frac{1}{2\pi}\theta^2\right) \\ -\cos\left(\frac{1}{2\pi}\theta^2\right) \end{pmatrix}. \tag{8}$$

We computed the Fourier transform of these fields according to Eqs. (3) and (4), to obtain the respective weights $C_k^2 = c_{s_k}^2 + c_{p_k}^2$, where c_s and c_p stand for the weights of the Fourier transforms of the fields $E_s(r, \theta)$ and $E_p(r, \theta)$, respectively. Results are shown in Fig. 7.

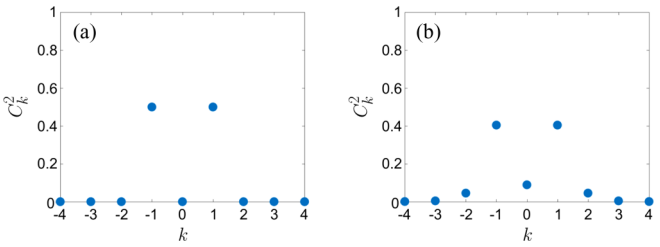

FIG. 7. Normalized weights $C_k^2 = c_{s_k}^2 + c_{p_k}^2$ of the terms in the Fourier transforms of the fields created with polynomial generalized q-plates with $q = 1/2$ when the input beam is vertically polarized. (a) Linear case ($p = 1$). (b) Nonlinear case ($p = 2$).

In the case $p = 1$ the only nonzero terms are $k = 1$ and $k = -1$; both terms and the sum of them are shown in Fig. 8. This, as expected, is identical to the field shown in Fig. 4. On the other hand, in the case with $p = 2$, while terms $k = 1$ and $k = -1$ remain the most significant, other terms arise, in particular that with $k = 0$. This term contributes with the Bessel function J_0, giving nonzero intensity at the propagation axis and hence destroying the dark singularity, as shown in Fig. 9. Since at the beam axis the only nonzero term is $k = 0$, the polarization there is linear at $-55°$. In the outer region, the predominant terms $k = 1$ and $k = -1$ create a cylindrically polarized vector beam. The continuous transition between the SoP at the center and in the outer region, and the phase difference between these terms due to the factor $(-i)^k$ in Eq. (4), forces the apparition of two C-points. It is worth mentioning why the field in Fig. 9(b) differs from that in Fig. 8(c). Even though they are both sums of terms with $k = -1$ and $k = 1$ with equal weighting, in the nonlinear case the Fourier decomposition of the vertical component $E_p(r, \theta)$ gives higher weight to these terms respect to other k values than the decomposition for the horizontal component $E_s(r, \theta)$. This results in higher intensity for the vertically polarized light when terms with $k = -1$ and $k = 1$ are added, hence breaking the cylindrical symmetry.

It is interesting to analyze how these fields evolve from their pass through the generalized q-plate to the far-field regime and how is the transition between the central singularity and the multiple isolated singularities. For that purpose we have simulated the device depicted in Fig. 10. We have added a quadratic phase to the field, representing the effect of a lens, and numerically calculated the Fresnel diffraction integral for

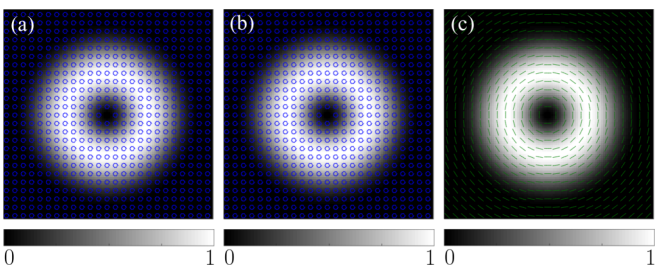

FIG. 8. Intensity and polarization patterns of Fourier transform terms of a field created with a polynomial generalized q-plate with $q = 1/2$ and $p = 1$, for vertically polarized input light. (a) Term with $k = -1$. (b) Term with $k = 1$. (c) Sum of both terms.

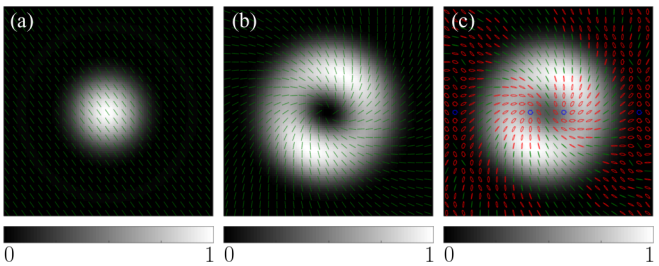

FIG. 9. Intensity and polarization patterns of Fourier transform terms of a field created with a polynomial generalized q-plate with $q = 1/2$ and $p = 2$, for vertically polarized input light. (a) Term with $k = 0$. (b) Sum of terms with $k = -1$ and $k = 1$. (c) Sum of terms with $k = -1$, $k = 0$, and $k = 1$.

transverse planes at different distances z, from the lens plane $z = 0$ to the focus $z = \mathbf{f}$. The field distribution at the focal plane is equal to that obtained by directly Fourier transforming (Fraunhofer diffraction). Intermediate planes show the beam polarization structure in the near-field regime.

Figure 11 shows some of the propagated fields for the case $q = 1/2$ and $p = 2$, when the input beam is vertically polarized. A short movie showing the complete evolution is included in the Supplemental Material [24]. For distances close to the lens plane, i.e., when $z < \mathbf{f} - \mathbf{f}/2$, the intensity of the beam remains approximately constant, and the polarization structure is the same as that in the generalized q-plate plane, with a central singularity; this is in agreement with the results reported in Ref. [16]. For $z = \mathbf{f} - \mathbf{f}/8$ the polarization field begins to distort, showing regions in which polarization is elliptical. Further on, e.g., when $z = \mathbf{f} - \mathbf{f}/32$, two critical points of the form factor clearly appear, in the center of the beam, and the central singularity is divided in two, although most of the polarization structure remains similar to that at $z = 0$. Finally at the focal plane the polarization structure is totally distorted, showing elliptic polarization around two C-points with a topological charge of $1/2$ and no central point with null intensity. It is remarkable that the SoP, which in principle does not show any symmetry, in the far-field regime gains symmetry with respect to the transformation that rotates the beam π radians around its axis and inverts the rotation of the polarization vector. When the input polarization is left (right) circular, the polarization turns right (left) circular and remains uniform during propagation. The phase distribution

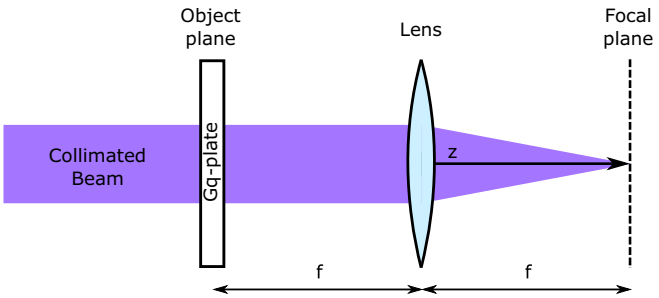

FIG. 10. Scheme of the optical device used for computing the beam evolution as it propagates from the generalized q-plate to the far-field regime.

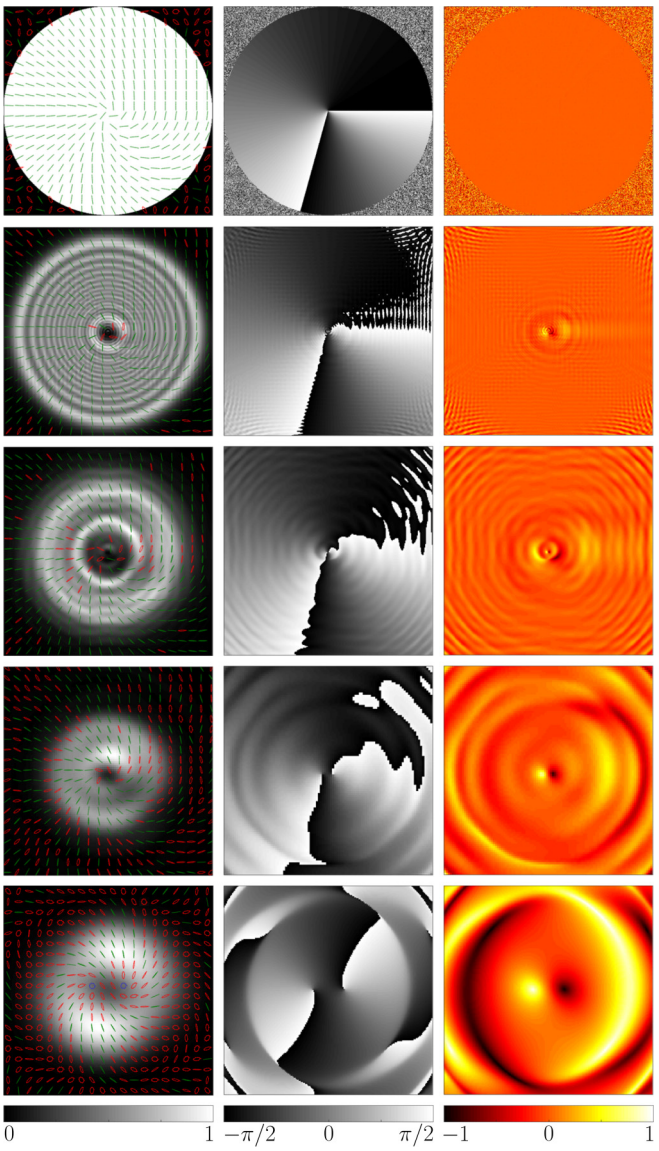

FIG. 11. Fresnel diffraction pattern at different planes resulting from a polynomial generalized q-plate with $q = 1/2$ and $p = 2$, when the input light is vertically polarized. The intensity distribution superposed to the polarization ellipses is shown in the first column. The azimuth and the form factor are depicted in the second and third columns, respectively. Rows show the evolution in the z coordinate, for $z = 0$, $z = \mathbf{f} - \mathbf{f}/2$, $z = \mathbf{f} - \mathbf{f}/8$, $z = \mathbf{f} - \mathbf{f}/32$, and $z = \mathbf{f}$, respectively.

remains unmodified for distances close to the lens plane and then distorts into the singularities discussed earlier.

B. Sinusoidal variation

Another possibility is that of designing an element that modulates the electric field without adding any net topological charge, e.g., a generalized q-plate defined by an oscillating function in θ. That is the case for the function $\Phi(\theta) = -(\pi/2)(\cos(q\theta) - 1)$, where 2Φ [Eq. (2) matrix argument] oscillates between 0 and 2π, q being the number of periods for $\theta \in [0, 2\pi]$. Figure 12 shows some examples of this function for different values of q.

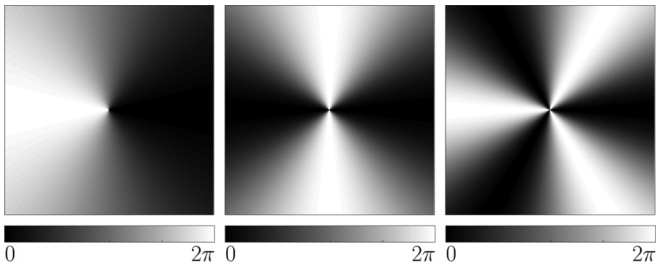

FIG. 12. Argument function $[2\Phi(r, \theta)]$ for sinusoidal generalized q-plates with $q = 1$, $q = 2$, and $q = 3$, respectively.

Figure 13 shows the results obtained from some of these generalized q-plates when vertically and left circularly polarized beams are used to illuminate the element. For a vertically polarized input, an output with uniform phase distribution and oscillating polarization azimuth is obtained, while for a circularly polarized input an oscillating phase distribution with uniform polarization is obtained. Again, as discussed in the previous section, at the exit of the generalized q-plate the function Φ defines the polarization structure when impinging with linear polarization and the phase structure when impinging with circular polarization. Interesting effects occur in the far field beyond the generalized q-plate, as shown in Fig. 14. Figure 14 shows the Fraunhofer diffraction fields obtained after impinging onto this kind of generalized q-plate with vertically polarized light. Yellow contours delimit the minimum intensity areas, defined as the regions with less than 0.5% of maximum intensity.

An interesting behavior that depends on the parity of q can be observed. For odd q values, the diffraction pattern shows several intensity minima, which match with corresponding saddle points in the form factor, keeping the azimuth of the polarization ellipses according to the input beam (except for 90° rotations). On the other hand, for even q values, the form factor remains uniformly zero (linear polarization), while $2q$ dark azimuth singularities arise, which match with corresponding $2q$ intensity minima, distributed geometrically

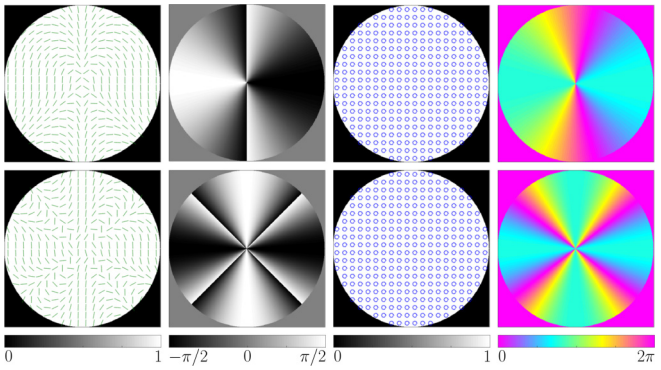

FIG. 13. Results provided by sinusoidal generalized q-plates with $q = 1$ (first row) and $q = 2$ (second row). The first column shows the intensity and polarization distribution for the vertical input polarization and the second column shows its respective azimuth. The third column shows the intensity and polarization distribution for the left circular input polarization and the fourth column shows its respective phase.

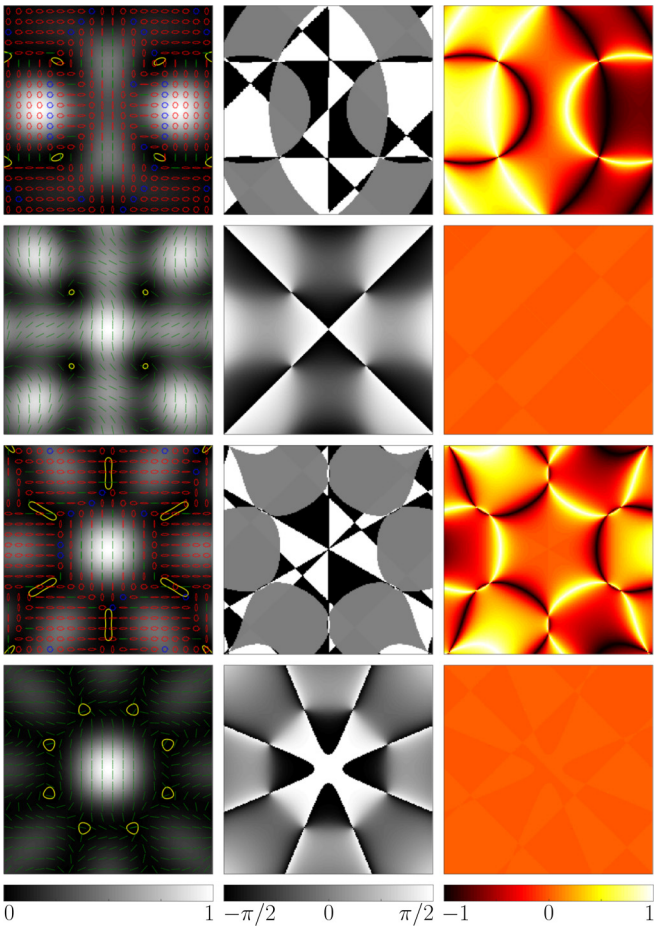

FIG. 14. Results for sinusoidal generalized q-plates in the far-field regime when the input polarization is vertical. The first column shows the polarization and intensity distribution, the second column shows the azimuth, and the third column shows the form factor. Rows show the cases for $q = 1$, $q = 2$, $q = 3$, and $q = 4$, respectively. Yellow lines demarcate minimum intensity areas.

around the beam axis. These singularities have alternate ± 1 topological charges, adding up to 0. The topological charge is measured as the times that the azimuth completes a 2π rotation along a closed path around the singularity, and the sing is provided by the sense of rotation; positive charge singularities are known as flowers, while negative charge singularities are known as webs [21].

This can be explained as well in terms of the Fourier transform decomposition of Eq. (4) discussed earlier. For instance, when the input light is vertically polarized, the electric field at the exit of the generalized q-plate is

$$\mathbf{E}_o(r,\theta) = \begin{pmatrix} E_s(r,\theta) \\ E_p(r,\theta) \end{pmatrix} = E_i \begin{pmatrix} \sin\{-\pi[\cos(q\theta) - 1]\} \\ -\cos\{-\pi[\cos(q\theta) - 1]\} \end{pmatrix}. \tag{9}$$

If we look at the c_k values of the Fourier transform of this field, it is found that for odd q values, E_s shows in its expansion only terms with odd k value, while E_p shows only even valued terms. Since all c_k values are real in this case, it means that the horizontal component of the electric field has the phase factor $(-i)^k = \pm i$, while the vertical component has the phase

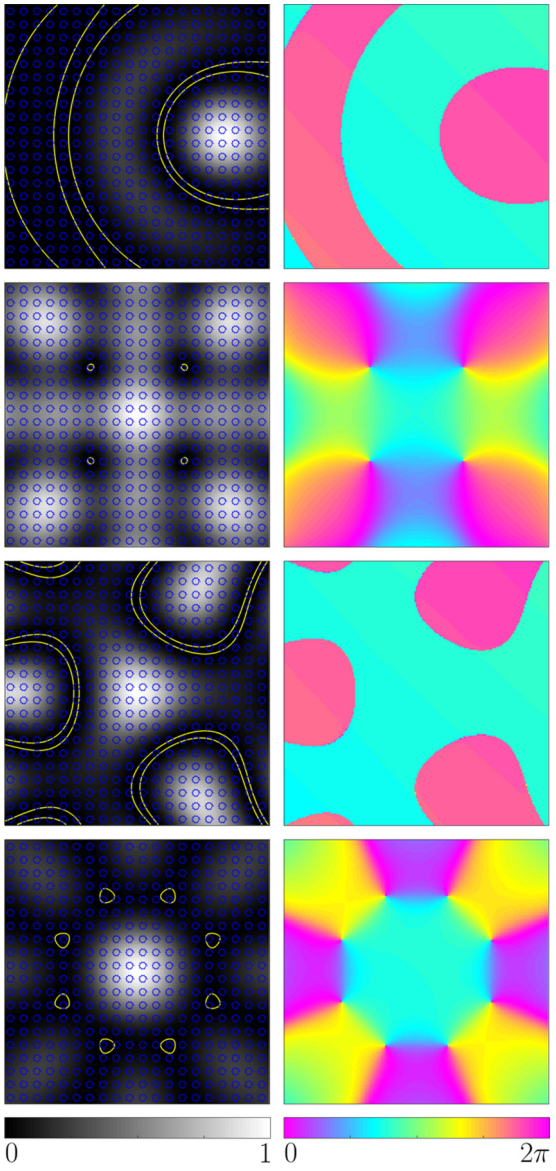

FIG. 15. Results for sinusoidal generalized q-plates in the far-field regime when the input polarization is left circular. The first column shows the intensity and polarization distribution, while the second column shows the phase distribution. Rows show the cases for $q = 1, q = 2, q = 3$, and $q = 4$, respectively. Yellow lines demarcate minimum intensity areas.

factor $(-i)^k = \pm 1$. Then, the phase difference between these components has to be $\pm\pi/2$, giving polarization ellipses that are vertically or horizontally oriented, with a form factor depending on the amplitude ratio. On the other hand, for even q values, Fourier expansion of both components of the electric field shows only terms with even k values, so the phase difference between them must be 0 or $\pm\pi$, now giving linear polarization with the azimuth depending on the amplitude ratio.

A similar distinction occurs when the polarization of the input beam is left circular, as shown in Fig. 15. For odd q values, there are no isolated singularities, but there are minima valleys which set a π step in the beam phase. Regarding Fig. 14 it

can be seen that these minima valleys match left circularly polarized regions resulting from a vertically polarized input. A vertically polarized beam can be described as the balanced superposition of left and right circularly polarized beams, and after passing through the generalized q-plate, the left circular polarization turns right, and vice versa. Then, it is reasonable that when the input light is left circularly polarized, regions of the output beam corresponding to left circular maxima show no intensity. On the other hand, for even q values there are $2q$ phase vortices carrying alternate topological charges (OAM) of ± 1, matching respective intensity isolated minima. Again, the total topological charge adds up to 0. Comparing with the case with a linearly polarized input, intensity distributions are the same, changing polarization vortices into phase vortices now. This is consistent, since sinusoidal generalized q-plates with even q values seem to modulate left and right circularly polarized light in the same way. This kind of distribution of optical vortices with alternate charges around the beam axis may have potential application in optical trapping and micromanipulation [25].

III. PROPOSED DEVICE TO MIMIC A GENERALIZED q-PLATE

Beyond studying the effects achieved by these alternative kinds of devices it is essential to provide an effective and efficient method for experimental implementation, which is vital for exploring new applications.

q-plates are typically inhomogeneous and anisotropic devices where effects like STOC are related to the Pancharatnam-Berry phase [26]. Here instead we propose a compact device that makes use of the propagation phase modulation provided by a phase-only SLM for emulating the effect of the generalized q-plates described above. The device is designed for modulating independently the phase of the orthogonal components of an input electric field, using a commercially available parallel-aligned reflective liquid crystal on silicon (PA-LCoS) display. This kind of display introduces a programmable phase modulation to one linear component of the field (let us suppose that the director of the LC molecules is horizontally oriented). The proposed setup is sketched in Fig. 16 and is based on a similar architecture used to encode q-plates by Moreno *et al.* [16]. There, the authors employ a parallel-aligned transmission display, which is an unusual device.

Let us describe how to get the desired modulation with this setup. The incident collimated beam passes through a first quarter-wave plate (QWP1) oriented at 45° and is reflected by means of a first beam-splitter (BS) onto one half of the LCoS, where a phase of $\psi = 2\Phi(r, \theta)$ is added to the horizontal component of the electric field. Then the beam propagates along a 4f system, where a quarter-wave plate (QWP2) oriented at 45° respect to the LC director, rotates the polarization vector in $-\pi/2$, due to the double passage caused by reflecting the beam with a mirror (M) located at the focus of L1. On the other half of the LCoS, the phase $-\psi = -2\Phi(r, \theta)$ is added to the remaining orthogonal component, and by means of a second beam-splitter, the reflected modulated beam goes through a third quarter-wave plate (QWP3) oriented at −45° and towards a CCD. Lens L2 is useful for measuring the output beam at different propagation distances, between near- and far-field regimes, it can be removed for observing directly the intensity obtained at the exit of the device.

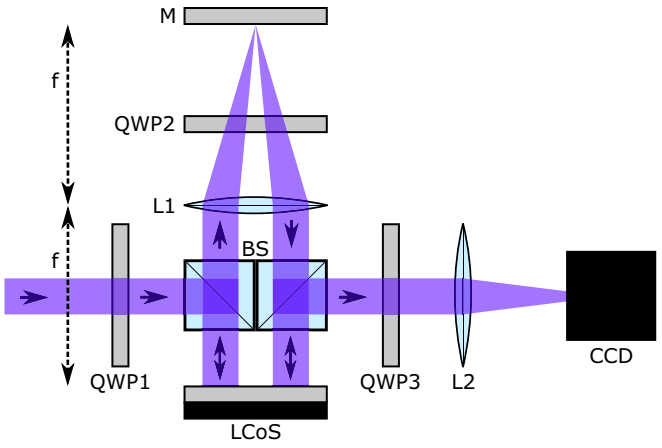

FIG. 16. Experimental compact device proposed for emulating generalized q-plates using a reflective PA-LCoS.

Although this device is not related directly to the Pancharatnam-Berry phase, its matrix representation coincides with that of the generalized q-plate [Eq. (2)], up to a global phase factor, then emulating all the expected behaviors. On the other hand, since it is possible to program it pixel by pixel, it allows one to make modifications at video rates, adding flexibility in the design of the mimicked plates and allowing an efficient and dynamic testing of these devices without requiring its fabrication.

IV. CONCLUSIONS

We simulated generalized q-plates which modulate the incident beam with nonlinear functions of the azimuthal variable and studied their effects on uniform linearly and circularly polarized beams. Furthermore, we proposed an experimental device capable of implementing these alternative kinds of devices in a dynamic and efficient way.

In the near-field approximation it is found that for a linearly polarized input, the output polarization structure is given by the argument function of the generalized q-plate, showing a central singularity, characteristic of conventional vector beams, while for a circularly polarized input the output phase structure is the one modulated, giving rise to the generation of OAM and the inversion of the polarization sense (STOC phenomenon).

In the far-field regime, it is found that when losing linearity in the azimuthal variable, the conventional central singularity divides into several singularities of minimum topological charge. In the cases where the input light is linearly polarized, the output beam can exhibit, either C-points with topological charges of $\pm 1/2$, as well as other types of critical points of the form factor, or dark polarization singularities (flowers and webs). Circularly polarized input beams result in the appearance of phase vortices, carrying OAM with a topological charge of ± 1. The intensity profiles and singularity distributions in each case depend on the particular chosen function Φ, giving the chance to model distributions of any

optical singularity known. These results were analyzed and discussed in terms of Fourier decomposition for separable functions in cylindrical coordinates.

Since the list of q-plate-based applications is extensive and still in growth [26], we think generalized q-plates based on arbitrary functions, together with the capability of representing these functions by means of an experimental device based on a PA-LCoS, which gives flexibility to the creation and manipulation of alternative kinds of vector and vortex beams, open a wide range of possibilities for experimental research of distributions of intensity, phase, and polarization, as well as singularities or critical points of different kinds, which are expected to have potential applications, e.g., in the field of singular optics and optical tweezers.

ACKNOWLEDGMENTS

This work was supported by UBACyT Grant No. 20020170100564BA and ANPCYT Grant No. PICT 2014/2432. M.V. holds a CONICET Fellowship.

[1] Q. Zhan, *Vectorial Optical Fields: Fundamentals and Applications* (World Scientific, Singapore, 2013).
[2] Q. Zhan, Adv. Opt. Photonics **1**, 1 (2009).
[3] S. Quabis, R. Dorn, M. Eberler, O. Glöckl, and G. Leuchs, Opt. Commun. **179**, 1 (2000).
[4] W. Cheng, J. W. Haus, and Q. Zhan, Opt. Express **17**, 17829 (2009).
[5] M. Woerdemann, C. Alpmann, M. Esseling, and C. Denz, Laser Photonics Rev. **7**, 839 (2013).
[6] Q. Zhan, Opt. Express **12**, 3377 (2004).
[7] H. Kawauchi, K. Yonezawa, Y. Kozawa, and S. Sato, Opt. Lett. **32**, 1839 (2007).
[8] Y. Zhao, Q. Zhan, Y. Zhang, and Y. Li, Opt. Lett. **30**, 848 (2005).
[9] M. Duocastella and C. Arnold, Laser Photonics Rev. **6**, 607 (2012).
[10] C. Gabriel, A. Aiello, W. Zhong, T. G. Euser, N. Y. Joly, P. Banzer, M. Förtsch, D. Elser, U. L. Andersen, C. Marquardt, P. S. J. Russell, and G. Leuchs, Phys. Rev. Lett. **106**, 060502 (2011).
[11] F. Cardano, E. Karimi, S. Slussarenko, L. Marrucci, C. de Lisio, and E. Santamato, Appl. Opt. **51**, C1 (2012).
[12] L. Marrucci, C. Manzo, and D. Paparo, Appl. Phys. Lett. **88**, 221102 (2006).
[13] L. Marrucci, C. Manzo, and D. Paparo, Phys. Rev. Lett. **96**, 163905 (2006).
[14] L. Marrucci, E. Karimi, S. Slussarenko, B. Piccirillo, E. Santamato, E. Nagali, and F. Sciarrino, J. Opt. **13**, 064001 (2011).
[15] A. Hermerschmidt, S. Osten, S. Krüger, and T. Blümel, Proc. SPIE **6584**, 65840E (2007).
[16] I. Moreno, M. M. Sanchez-Lopez, K. Badham, J. A. Davis, and D. M. Cottrell, Opt. Lett. **41**, 1305 (2016).
[17] W. Ji, C. Lee, P. Chen, W. Hu, Y. Ming, L. Zhang, T. Lin, V. Chigrinov, and Y. Lu, Sci. Rep. **6**, 25528 (2016).
[18] J. E. Holland, I. Moreno, J. A. Davis, M. M. Sánchez-López, and D. M. Cottrell, Appl. Opt. **57**, 1005 (2018).
[19] M. Rafayelyan and E. Brasselet, Opt. Lett. **42**, 1966 (2017).
[20] I. Moreno, M. Yzuel, J. Campos, and A. Vargas, J. Mod. Opt. **51**, 2031 (2004).
[21] I. Freund, M. Soskin, and A. I. Mokhun, Opt. Commun. **208**, 223 (2002).
[22] M. Padgett and R. Bowman, Nat. Photonics **5**, 343 (2011).
[23] J. W. Goodman, *Introduction to Fourier Optics* (McGraw-Hill, New York, 1996).
[24] See Supplemental Material at http://link.aps.org/supplemental/10.1103/PhysRevA.100.053812 for a short movie showing the complete evolution of a beam propagating from the generalized q-plate plane to the far-field regime.
[25] M. Gecevicius, R. Drevinskas, M. Beresna, and P. Kazansky, Appl. Phys. Lett. **104**, 231110 (2014).
[26] A. Rubano, F. Cardano, B. Piccirillo, and L. Marrucci, J. Opt. Soc. Am. B **36**, D70 (2019).